Int. J. Electrochem. Sci., 15 **(2020)** 803 – 815, doi: 10.20964/2020.01.47

International Journal of
ELECTROCHEMICAL
SCIENCE
www.electrochemsci.org

Nb-doped $Li_{1.20}[Mn_{0.54}Ni_{0.13}Co_{0.13}]O_2$ Cathode Material with Enhanced Electrochemical Properties for Lithium-Ion Battery

*Yang Xu, Qingzhong Cui**

State Key Laboratory of Explosion Science and Technology, Beijing Institute of Technology, Beijing 100081, China.
*E-mail: qingzhongcui@foxmail.com

Received: 24 August 2019 / *Accepted:* 18 October 2019 / *Published:* 30 November 2019

To enhance the electrochemical properties and structure stability of the Layered Li-rich Mn-based oxides, the Nb^{5+} with different contents were doped into the $Li_{1.20}[Mn_{0.54}Ni_{0.13}Co_{0.13}]O_2$ via using the carbonate co-precipitation method. The effect of the Nb^{5+} doping modification on the microstructure, morphology and electrochemical properties of the $Li_{1.20}[Mn_{0.54}Ni_{0.13}Co_{0.13}]O_2$ cathode have been investigated by the XRD, SEM, XPS, galvanostatic discharge-charge tests and electrochemical impedance spectroscopy (EIS) techniques. The results demonstrated the Nb^{5+} doping not only could enhance the cation order degree, but also contributed to enhancing the Li^+ migration speed during cycling. The $Li_{1.20}[Mn_{0.54}Ni_{0.13}Co_{0.13}]_{0.78}Nb_{0.02}O_2$ delivered about 20.6 mAh g^{-1} larger than that of the pristine one at 5C high rate. In addition, the $Li_{1.20}[Mn_{0.54}Ni_{0.13}Co_{0.13}]_{0.78}Nb_{0.02}O_2$ retained a much higher discharge capacity retention of 92.5% after 100 cycles. Whereas, the pristine cathode showed only 85.7% of the capacity retention under identical conditions. These results indicated that Nb^{5+} doping modification could effectively enhance the electrochemical properties of $Li_{1.20}[Mn_{0.54}Ni_{0.13}Co_{0.13}]O_2$.

Keywords: $Li_{1.20}[Mn_{0.54}Ni_{0.13}Co_{0.13}]O_2$; Nb^{5+} doping; High cation ordering; Superior rate capacity; Cyclic stability.

1. INTRODUCTION

Lithium ion batteries have been widely used in portable devices, energy storage devices and other fields [1, 2]. And with the development of electric vehicle and hybrid vehicle industry, the energy density of traditional cathode materials for lithium ion battery, such as layered $LiCoO_2$[3], spinel $LiMn_2O_4$ [4], olivine $LiFePO_4$ [5] and layered $LiMn_{1/3}Ni_{1/3}Co_{1/3}O_2$ [6], has been unable to meet the basic needs of this field. Therefore, to explore the outstanding performance cathode materials has become the innovation and research focus [7-8]. Recently, the Layered Li-rich and Mn-based oxides have appealed to much attention owing to the high discharge capacity (>280 mAh g^{-1}) and high energy density, which have been

regarded as an attracted candidate cathode for the new generation of high capacity Li-ion batteries [9-11].

However, the Layered Li-rich and Mn-based oxides have still presented some intrinsic drawbacks, including the large initial irreversible capacity loss, unsatisfactory discharge capacities at high rate and severe capacity degradation during cycling owing to the cation mixing between Ni^{2+} and Li^{+} [12-15]. And many improving programs have demonstrated the ion doping can effectively reduce the mixing effect of cation [16-18]. Besides, *J. Lee et al.* have synthesized the Li_2MnO_3 cathode material via Nb^{5+} and F^{-} doping, and the related results have been published on *Nature* in 2018 [19]. The $Li_2Mn_{2/3}Nb_{1/3}O_2F$ cathode material demonstrated the outstanding electrochemical properties owing to the slightly structural change and oxygen loss of $Li_2Mn_{2/3}Nb_{1/3}O_2F$ cathode during cycling. Inspired by the idea, the Layered Li-rich and Mn-based oxides $0.6Li_2MnO_3{\cdot}0.4LiMn_{1/3}Ni_{1/3}Co_{1/3}O_2$ ($Li_{1.20}[Mn_{0.54}Ni_{0.13}Co_{0.13}]O_2$) doped by Nb^{5+} may be a good choice to enhance the electrochemical performance.

In this paper, the $Li_{1.20}[Mn_{0.54}Ni_{0.13}Co_{0.13}]_{0.8-x}Nb_xO_2$ (x = 0, 0.01, 0.02, 0.03) were synthesized by carbonate co-precipitation method, followed by high temperature solid phase method. And the XRD, SEM, XPS and EIS measurements were used to identify the effect of Nb^{5+} doping on the morphology and microstructure of cathode. Besides, the 1st coulombic efficiency, rate capacities, and cycling performance were also studied scientifically.

2. EXPERIMENTAL

2.1 Materials preparation

Firstly, $[Mn_{0.54}Ni_{0.13}Co_{0.13}](CO_3)_{0.8}$ served as the precursor of $Li_{1.20}[Mn_{0.54}Ni_{0.13}Co_{0.13}]_{0.8-x}Nb_xO_2$ (x = 0, 0.01, 0.02, 0.03) was synthesized by a carbonate co-precipitation method [20]. The solution of $NiSO_4{\cdot}6H_2O$, $CoSO_4{\cdot}7H_2O$ and $MnSO_4{\cdot}H_2O$ (in corresponding molar ratio of 0.54: 0.13: 0.13) was dropped into a continuous stirred tank reactor filled with N_2. Meanwhile, the property amounts of Na_2CO_3 and $NH_3{\cdot}H_2O$ solution were respectively added into the mixed solution to control the pH value of the solution at 8.0. Lastly, the precipitate slurry was segregated, washed and dried at 100 ºC for 10 h to acquire $[Mn_{0.54}Ni_{0.13}Co_{0.13}](CO_3)_{0.8}$.

To prepare the $Li_{1.20}[Mn_{0.54}Ni_{0.13}Co_{0.13}]_{0.8-x}Nb_xO_2$ (x = 0, 0.01, 0.02, 0.03) cathode materials, the suitable ratio of $[Mn_{0.54}Ni_{0.13}Co_{0.13}](CO_3)_{0.8}$, $LiOH{\cdot}H_2O$ and Nb_2O_5 were mixed well with ball milling. Then the compound was sintered at 550 ºC for 6 h, followed by elevated to 900 ºC for 10 h in air to obtain the target cathode materials.

2.2 Material characterizations

The chemical composition of $Li_{1.20}[Mn_{0.54}Ni_{0.13}Co_{0.13}]_{0.8-x}Nb_xO_2$ (x = 0, 0.01, 0.02, 0.03) were monitored by ICP-OES (Inductively Coupled Plasma Optical Emission Spectrometer, iCAP 6000). The micro-structure of $Li_{1.20}[Mn_{0.54}Ni_{0.13}Co_{0.13}]_{0.8-x}Nb_xO_2$ (x = 0, 0.01, 0.02, 0.03) were measured by Rigaku

RINT2400 X-ray diffractometer using Cu Kα radiation. The XRD data was collected in the range of 10º~80º with a step size of 0.01º and a count time of 5.0s. And the XRD data were refined by Rietveld method using the FULLPROF software. The morphologies of the cathode materials were observed by a scanning electron microscope (SEM, JEOL JSM-6510LV). The valence state of doped Nb^{5+} was analyzed by X-ray photoelectron spectroscopy (XPS, Thermo Scientific ESCALAB 250Xi), with Al Kα source at 14.0 kV and 25 mA.

2.3 Electrochemical tests

The cathode electrode was prepared according to the mass ratio of cathode active material: acetylene black: PVDF = 8:1:1. Then the prepared cathode, lithium metal as the anode and a micro porous membrane (Celgard 2320) as a separator were assembled in an argon-filled glove box to form the CR2025 coin-type cells. The electrolyte solution was a 1 mol L^{-1} $LiPF_6$ in ethylene carbonate (EC)/dimethyl carbonate (DMC) solution. The Galvanostatic charge-discharge tests were measured by BTS series battery testing system between 2.0 and 4.8 V at 25℃. Electrochemical impedance spectroscopy (EIS) test was conducted by PARSTAT M2273 electrochemical workstation between 0.01 Hz to 100 kHz with an amplitude of 5 mV.

3. RESULTS AND DISCUSSION

Table1 shows the Mn, Ni, Co and Nb compositions of $Li_{1.20}[Mn_{0.54}Ni_{0.13}Co_{0.13}]_{0.8-x}Nb_xO_2$ (x = 0, 0.01, 0.02, 0.03). The ICP test results demonstrate that the molar ratio of Mn: Ni: Co: Nb of all cathode materials have been conformed to the experimental design values.

Table 1. The Mn, Ni, and Co, Nb compositions of $Li_{1.20}[Mn_{0.54}Ni_{0.13}Co_{0.13}]_{0.8-x}Nb_xO_2$ (x = 0, 0.01, 0.02, 0.03).

Sample	Theoretical molar ratio				Measurement molar ratio			
	Mn	Ni	Co	Nb	Mn	Ni	Co	Nb
x = 0	0.540	0.130	0.130	0	0.540	0.129	0.131	0
x = 0.01	0.534	0.128	0.128	0.010	0.532	0.128	0.129	0.011
x = 0.02	0.524	0.127	0.127	0.020	0.526	0.125	0.126	0.021
x = 0.03	0.520	0.125	0.125	0.030	0.519	0.124	0.126	0.031

Fig.1 shows the XRD patterns of $Li_{1.20}[M\ n_{0.54}Ni_{0.13}Co_{0.13}]_{0.8-x}Nb_xO_2$ (x = 0, 0.01, 0.02, 0.03). The as-prepared cathodes have mainly been indexed to the typical XRD patterns of the hexagonal α-$NaFeO_2$ structure with the space group R-3m ($LiNi_{1/3}Co_{1/3}Mn_{1/3}O_2$ phase), except for the weak super lattice peaks from 20° to 25°, which belongs to the Li_2MnO_3 phase with the monocline unit cell C2/m [21, 22]. And the obvious splitting peaks of (108)/(110) and (006)/((102) implies that the synthesized cathode materials demonstrate a well layered structure [23]. To further analyze the Li/Ni exchange of

all samples, the Rietveld refinement of the diffraction patterns are carried out based on the R-3m space group, and the main structural parameters as a hexagonal setting are demonstrated in Table 2.

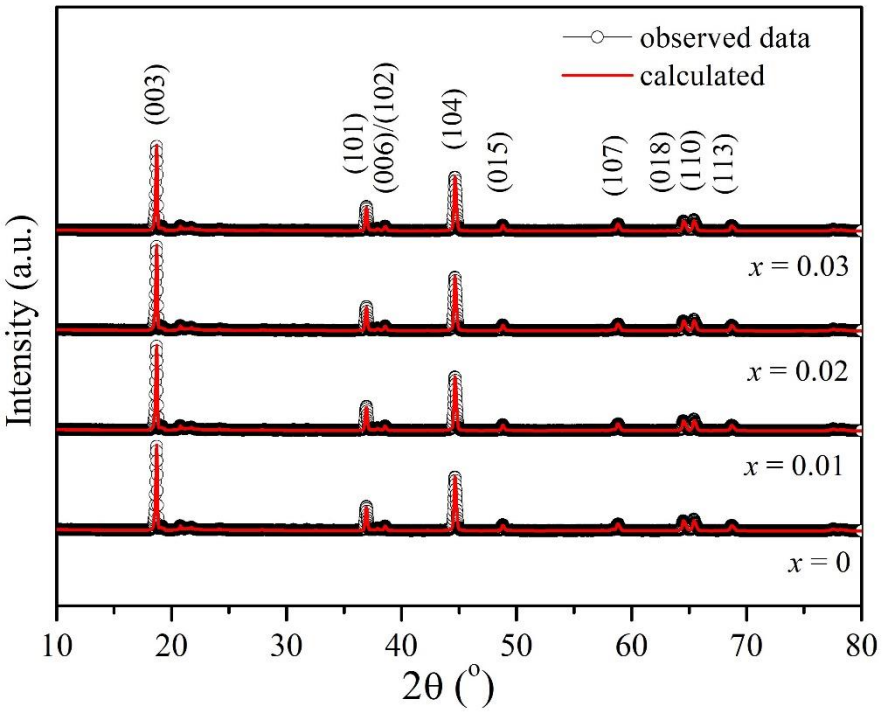

Figure 1. Rietveld refined patterns of $Li_{1.20}[Mn_{0.54}Ni_{0.13}Co_{0.13}]_{0.8-x}Nb_xO_2$ (x = 0, 0.01, 0.02, 0.03).

Table 2. Refined structural data for $Li_{1.20}[Mn_{0.54}Ni_{0.13}Co_{0.13}]_{0.8-x}Nb_xO_2$ (x = 0, 0.01, 0.02, 0.03).

Sample	a(Å)	c(Å)	c/a	Ni_{3a}/Ni_{tot} (%)	R_p(%)	R_{wp}(%)
x = 0	2.8485(1)	14.2102(2)	4.9887	10.3	7.5	8.3
x = 0.01	2.8503(1)	14.2245(2)	4.9905	8.92	7.9	8.6
x = 0.02	2.8541(1)	14.2462(1)	4.9915	6.85	9.2	8.2
x = 0.03	2.8563(1)	14.2553(1)	4.9908	7.28	8.7	7.6

It can be seen that the lattice parameters of c and a gradually enlarge with the increase of Nb^{5+} doping amounts. And the c/a ratio of all cathodes are larger than 4.98, suggesting the formation of the well layered structure [24]. Besides, the cation mixing between Li^+ and Ni^{2+} due to the similar radius of Li^+ (0.076 nm) and Ni^{2+} (0.069 nm) will influence the structure stability of cathode during cycling [25]. The value of Ni_{3a}/Ni_{tot} in Table 2 stands for the cation mixing degree of Li^+ and Ni^{2+} site-exchange. With the Nb^{5+} doping amounts increasing, the percentage of Ni_{3a}/Ni_{tot} firstly decrease from 10.3%, 8.92% to 6.85%, and then enlarge to 7.28%, the $Li_{1.20}[Mn_{0.54}Ni_{0.13}Co_{0.13}]_{0.78}Nb_{0.02}O_2$ delivers the lowest degree of cation mixing. The results indicate that the substitution of Nb^{5+} for transition metal ions can effectively lower the cation mixing and restrain the structure degradation during cycling.

Fig.2 shows the SEM images of $Li_{1.20}[Mn_{0.54}Ni_{0.13}Co_{0.13}]_{0.8-x}Nb_xO_2$ (x = 0, 0.01, 0.02, 0.03). The synthesized samples are composed of isolated rock-shaped grains in the diameter of 200~800 nm, which demonstrate the clean surface and sharp edge without obvious aggregation.

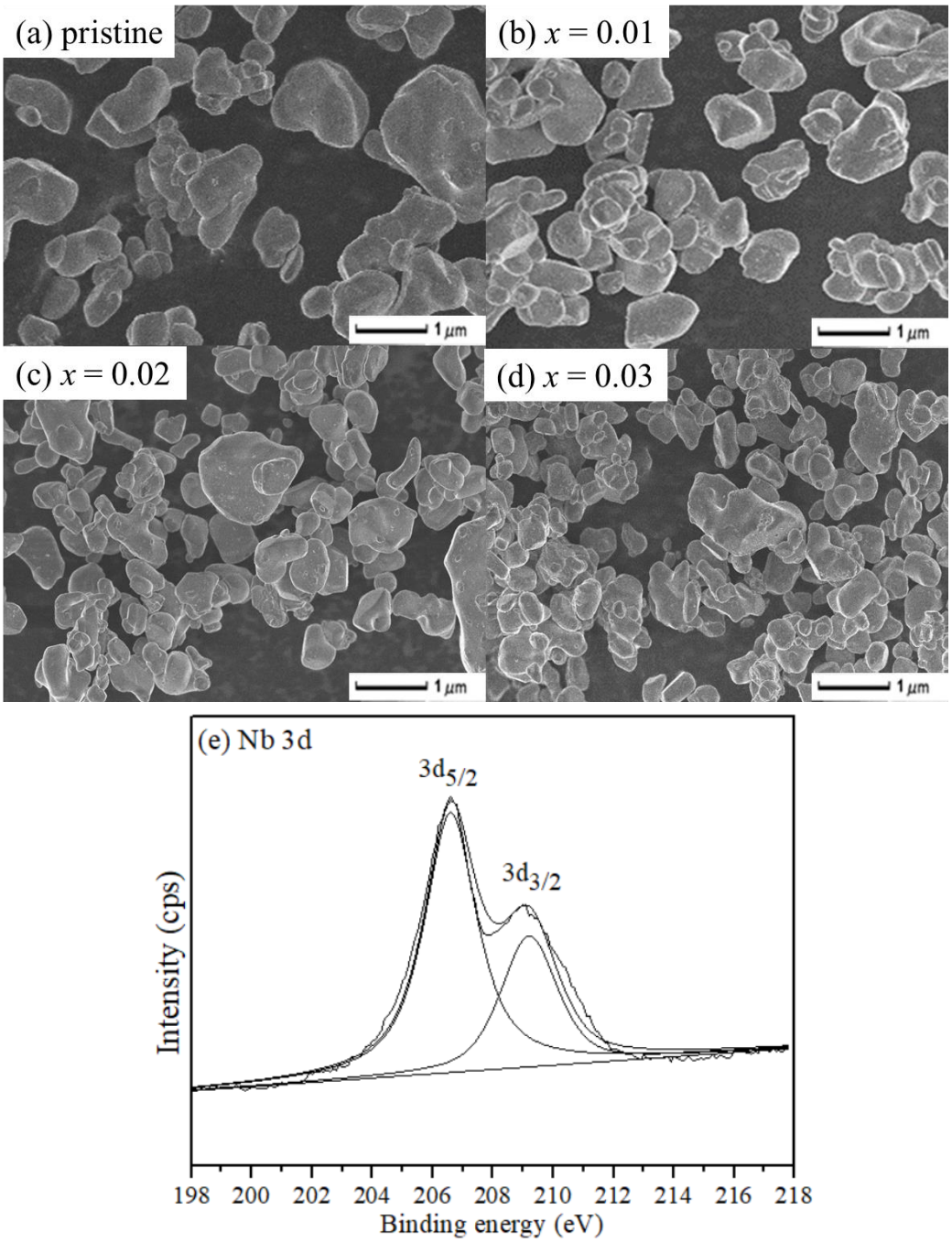

Figure 2. SEM images of $Li_{1.20}[Mn_{0.54}Ni_{0.13}Co_{0.13}]_{0.8-x}Nb_xO_2$ (x = 0, 0.01, 0.02, 0.03) (a-d) and XPS spectra of Nb 3d for $Li_{1.20}[Mn_{0.54}Ni_{0.13}Co_{0.13}]_{0.78}Nb_{0.02}O_2$.

It demonstrates all cathode particles present the high crystallinity. In addition, with the Nb^{5+} doping amounts increasing, the cathode particles sizes will reduce owing to the space steric effect of Nb_2O_5 [26], and the less size particles contribute to enhancing the Li^+ transmission ability and discharge capacity at high rate [27]. To study the chemical valence state of Nb doping element in the cathode, XPS

measurement of Nb 3d for $Li_{1.20}[Mn_{0.54}Ni_{0.13}Co_{0.13}]_{0.78}Nb_{0.02}O_2$ has been performed, as is shown in Fig.2(e). The two main obvious peaks are respectively assigned to Nb $3d_{3/2}$ and Nb $3d_{5/2}$, suggesting the doping Nb element is at the state of 5+ [27]. The result indicates the Nb^{5+} was successfully doped into $Li_{1.20}[Mn_{0.54}Ni_{0.13}Co_{0.13}]O_2$.

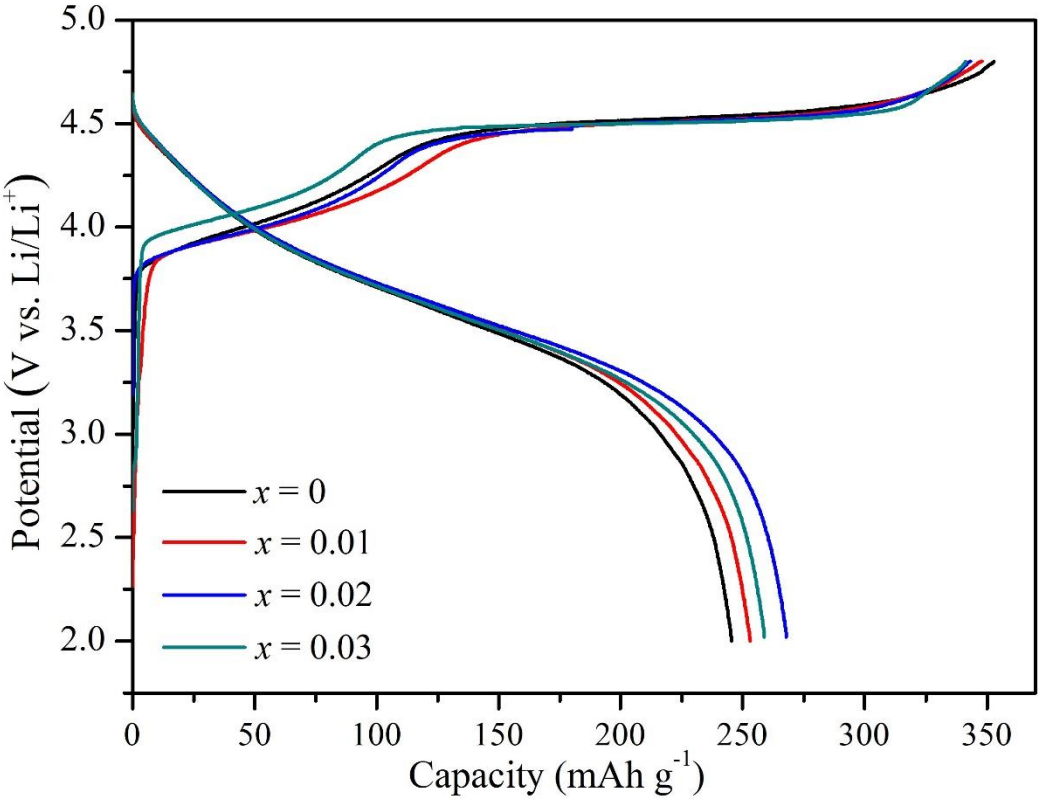

Figure 3. Initial charge and discharge curves of $Li_{1.20}[Mn_{0.54}Ni_{0.13}Co_{0.13}]_{0.8-x}Nb_xO_2$ (x = 0, 0.01, 0.02, 0.03) between 2.0V and 4.8V at 0.1 C rate.

Fig.3 shows the initial charge and discharge curves of $Li_{1.20}[Mn_{0.54}Ni_{0.13}Co_{0.13}]_{0.8-x}Nb_xO_2$ (x = 0, 0.01, 0.02, 0.03) between 2.0V and 4.8V at 0.1 C rate. It can be observed that all samples show a typical two-step profile during the initial charge process. The first plateau located at 2.0V~ 4.5 V can be attributed to extraction process of Li^+ from the $LiNi_{1/3}Co_{1/3}Mn_{1/3}O_2$ phase together with the oxidation of $Ni^{2+}\rightarrow Ni^{4+}$ and $Co^{3+}\rightarrow Co^{4+}$ [28, 29]. The second plateau above 4.5 V is correlative with the activation of Li_2MnO_3 component, corresponding to the irreversible extraction of Li^+ and O^{2-} (as Li_2O) from the Li_2MnO_3 [30, 31]. In comparison with the $Li_{1.20}[Mn_{0.54}Ni_{0.13}Co_{0.13}]O_2$, the $Li_{1.20}[Mn_{0.54}Ni_{0.13}Co_{0.13}]_{0.8-x}Nb_xO_2$ (x = 0.01, 0.02, 0.03) deliver the less initial charge capacities due to the electrochemical inactive of Nb^{5+}. Table 3 shows that with the Nb^{5+} doping amounts increasing, $Li_{1.20}[Mn_{0.54}Ni_{0.13}Co_{0.13}]_{0.8-x}Nb_xO_2$ (x = 0, 0.01, 0.02, 0.03) deliver the discharge specific capacities of 245.5, 253.0, 267.7 and 258.7mAh g^{-1} , respectively, corresponding that the initial coulombic efficiency is firstly enhancing from 69.6%, 72.7% to 78.0%, and then decreased to 75.8%. The results indicate that the Nb^{5+} doping can effectively suppress the irreversible extraction of Li^+ and O^{2-} from the Li_2MnO_3 and lower the migration of oxygen vacancies for that the bond dissociation energy of Nb-O is stronger than that of M-O (M = Mn, Ni, and Co) [32], which could restrain the oxygen escape from the Li_2MnO_3 lattice.

Table 3. Initial cycle electrochemical data of $Li_{1.20}[Mn_{0.54}Ni_{0.13}Co_{0.13}]_{0.8-x}Nb_xO_2$ (x = 0, 0.01, 0.02, 0.03) at 0.1C rate in the voltage range of 2.0~4.8 V.

Sample	Charge capacity (mAh g^{-1})	Discharge capacity (mAh g^{-1})	Irreversible capacity loss (mAh g^{-1})	Coulombic efficiency (%)
x = 0	352.8	245.5	107.3	69.6
x = 0.01	348.1	253.0	95.1	72.7
x = 0.02	343.2	267.7	75.5	78.0
x = 0.03	341.3	258.7	82.6	75.8

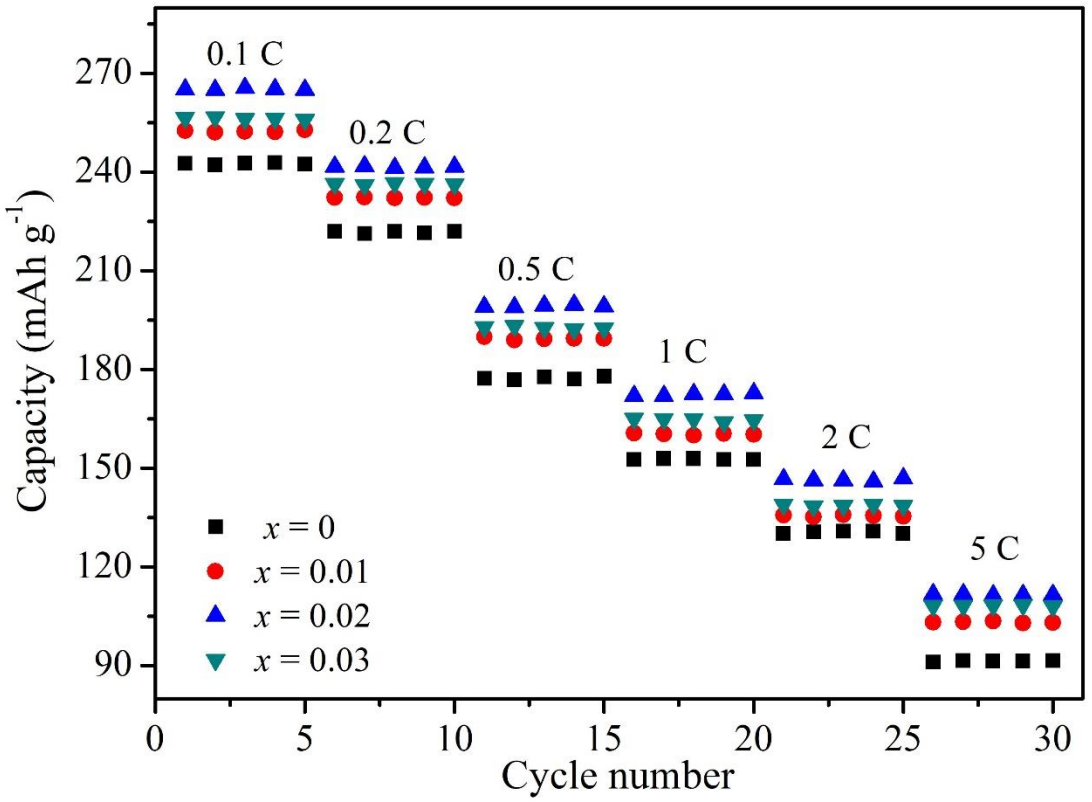

Figure 4. Discharge capacities of $Li_{1.20}[Mn_{0.54}Ni_{0.13}Co_{0.13}]_{0.8-x}Nb_xO_2$ (x = 0, 0.01, 0.02, 0.03) at various rates.

Fig.4 shows the discharge capacities of $Li_{1.20}[Mn_{0.54}Ni_{0.13}Co_{0.13}]_{0.8-x}Nb_xO_2$ (x = 0, 0.01, 0.02, 0.03) at various rates. It can be observed that all cathodes deliver the less and less discharge capacities with the discharge current density increasing owing to the ionic polarization influence [33]. In addition, the cathodes after Nb^{5+} doping have demonstrated the obvious enhanced discharge capacities than those of pristine cathode at any rates, as is shown in Table 4. And with the Nb^{5+} doping amounts enhancing, the discharge capacities of $Li_{1.20}[Mn_{0.54}Ni_{0.13}Co_{0.13}]_{0.8-x}Nb_xO_2$ (x = 0.01, 0.02, 0.03) firstly increase and then decline, especially the $Li_{1.20}[Mn_{0.52}Ni_{0.13}Co_{0.13}Nb_{0.02}]O_{1.95}F_{0.05}$ delivers the optimal rate capacities at every rate. Table 4 shows that the discharge capacities of pristine sample are severally 242.6, 221.9, 177.3, 152.6, 130.1 and 91.1 mAh g^{-1} at rates of 0.1, 0.2, 0.5, 1, 2, 5C, while $Li_{1.20}[Mn_{0.54}Ni_{0.13}Co_{0.13}]_{0.78}Nb_{0.02}O_2$ delivers the larger discharge capacities of 265.2, 241.7, 199.1,

172.2, 146.7 and 111.7mAh g^{-1}, accordingly. At the discharge rate of 5 C, the discharge capacity of the $Li_{1.20}[Mn_{0.54}Ni_{0.13}Co_{0.13}]_{0.78}Nb_{0.02}O_2$ is 20.6 mAh g^{-1} larger than that of pristine one. The results indicate that the Nb^{5+} doping can effectively enhance the rate capacity of $Li_{1.20}[Mn_{0.54}Ni_{0.13}Co_{0.13}]O_2$ for that the less size particles of Nb^{5+} doped cathodes could reduce the Li^+ migration path and the larger crystal lattice parameters by Nb^{5+} doping can also contribute to enhancing the Li^+ migration speed [34].

Table 4. Rate capacities of pristine $Li_{1.20}[Mn_{0.54}Ni_{0.13}Co_{0.13}]_{0.8-x}Nb_xO_2$ (x = 0, 0.01, 0.02, 0.03) at various current densities in the voltage range of 2.0-4.8 V.

sample	0.1C rate (mAh g^{-1})	0.2C rate (mAh g^{-1})	0.5C rate (mAh g^{-1})	1C rate (mAh g^{-1})	2C rate (mAh g^{-1})	5C rate (mAhg^{-1})
x = 0	242.6	221.9	177.3	152.6	130.1	91.1
x = 0.01	252.6	232.3	189.9	160.7	135.7	103.2
x = 0.02	265.2	241.7	199.1	172.2	146.7	111.7
x = 0.03	256.5	236.4	192.9	165.0	138.9	108.2

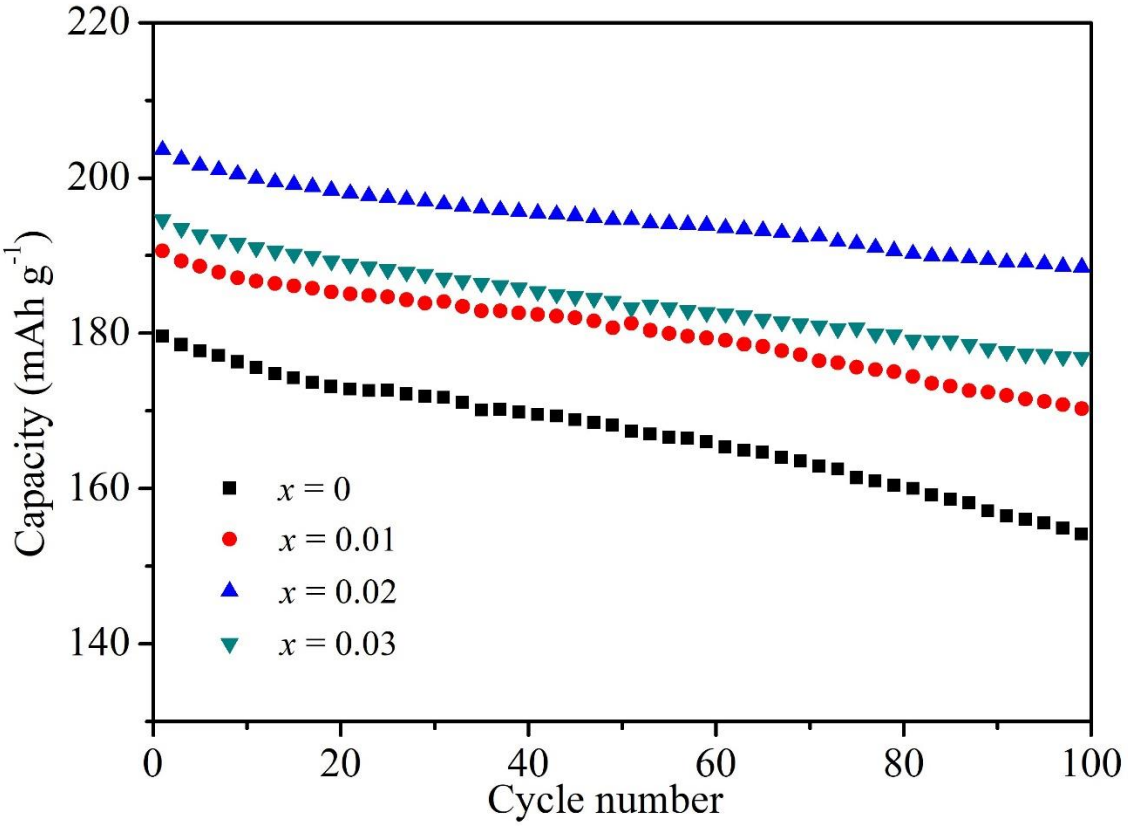

Figure 5. Cyclic performance of the $Li_{1.20}[Mn_{0.54}Ni_{0.13}Co_{0.13}]_{0.8-x}Nb_xO_2$ (x = 0, 0.01, 0.02, 0.03) at 0.5C rate.

Fig.5 shows the cyclic performance of the $Li_{1.20}[Mn_{0.54}Ni_{0.13}Co_{0.13}]_{0.8-x}Nb_xO_2$ (x = 0, 0.01, 0.02, 0.03) at 0.5C rate and room temperature. With the cycles going on, all samples have demonstrated the

attenuated discharge capacity. Notably the pristine cathode decays more rapidly during cycling, and its discharge capacities at the initial and 100th cycles are 179.6 and 153.9 mAh g^{-1}, respectively, corresponding to the capacity retention of 85.7%, as is seen in Table 5.

Table 5. Cyclic performance of pristine $Li_{1.20}[Mn_{0.54}Ni_{0.13}Co_{0.13}]_{0.8-x}Nb_xO_2$ (x = 0, 0.01, 0.02, 0.03) at 0.5 C rate in the voltage range of 2.0-4.8 V at 25°C.

Sample	Initial discharge specific capacity (mAh g^{-1})	100th Specific discharge capacity (mAh g^{-1}`)	100 cycles capacity retention (%)
x = 0	179.6	153.9	85.7
x = 0.01	190.6	170.2	89.3
x = 0.02	203.6	188.4	92.5
x = 0.03	194.6	176.8	90.9

While the cathodes after Nb^{5+} doping show an enhanced cyclic performance and higher capacity retention. With the Nb^{5+} doping amounts increasing, the capacity retentions of $Li_{1.20}[Mn_{0.54}Ni_{0.13}Co_{0.13}]_{0.8-x}Nb_xO_2$ (x = 0.01, 0.02, 0.03) after 100 cycles firstly enhance and then decrease, and the $Li_{1.20}[Mn_{0.54}Ni_{0.13}Co_{0.13}]_{0.78}Nb_{0.02}O_2$ delivers the optimal cyclic stability. It delivers a discharge capacity of 203.6 mAh g^{-1} at 1st cycle, and this value could still keep at 188.4 mAh g^{-1} after 100 cycles with a high capacity retention of 92.5%, much larger than that of the pristine sample. The enhanced cyclic performance for Nb^{5+} doped cathodes can be attributed to the high cation order and the stronger binding of Nb-O, which contributes to maintaining the structure stability during cycling [35]. However, when the doping content further enhances (x = 0.03), the cyclic performance of the as-prepared has declined on the contrary for that the excessive doping will lead to an increased cation mixing degree.

Table **6** shows the electrochemical properties of Zr^{4+}-doped $Li_{1.20}[Mn_{0.54}Ni_{0.13}Co_{0.13}]O_2$ [18], Mo^{6+}-doped $Li_{1.20}[Mn_{0.54}Ni_{0.13}Co_{0.13}]O_2$ [23] and Ca^{2+}-doped $Li_{1.20}[Mn_{0.54}Ni_{0.13}Co_{0.13}]O_2$ [36] when compared with $Li_{1.20}[Mn_{0.54}Ni_{0.13}Co_{0.13}]_{0.78}Nb_{0.02}O_2$ in the work. The Nb^{5+} doped cathode delivers the obvious less discharge capacity than those of Zr^{4+}, Mo^{6+} and Ca^{2+} doped cathodes. It may be attributed that the Zr^{4+}, Mo^{6+} and Ca^{2+} doping modification can obviously enlarge the interplanar spacing and reduce activation barrier for Li^+ diffusion. However, when compared with the Zr^{4+}, Mo^{6+} and Ca^{2+} doped cathodes, the Nb^{5+} doping modification has demonstrated the superior cyclic performance due to the high structure stability.

Table 6. The electrochemical properties comparison of some similar cathode materials.

Cathode	1st Coulombic efficiency (%)	Discharge capacity at 2C rate (mAh g^{-1})	Cyclic performance (%)
Zr^{4+} doping [18]	79.1	145.6	90.4
Mo^{6+} doping [23]	81.3	192.0	81.8
Ca2+ doping [36]	82.5	180.0	86.8
Nb^{5+} doping	78.0	146.7	92.5

Table 7. The simulated data of $Li_{1.20}[Mn_{0.54}Ni_{0.13}Co_{0.13}]_{0.8-x}Nb_xO_2$ (x = 0, 0.01, 0.02, 0.03) at 4.5 V from EIS spectra using the equivalent circuit shown in Fig. 6(e).

Sample	Cycle number	R_s (Ω)	R_{sf} (Ω)3	R_{ct}(Ω)	$\triangle R_{ct}$(Ω)
x = 0	1st	20.5	33.6	175.3	423.0
	100th	53.4	87.5	598.3	
x = 0.01	1st	16.8	29.8	158.6	330.7
	100th	41.8	71.8	489.3	
x = 0.02	1st	11.5	25.4	134.5	261.2
	100th	32.6	58.9	395.7	
x = 0.03	1st	14.1	27.8	148.6	289.6
	100th	38.7	65.7	438.2	

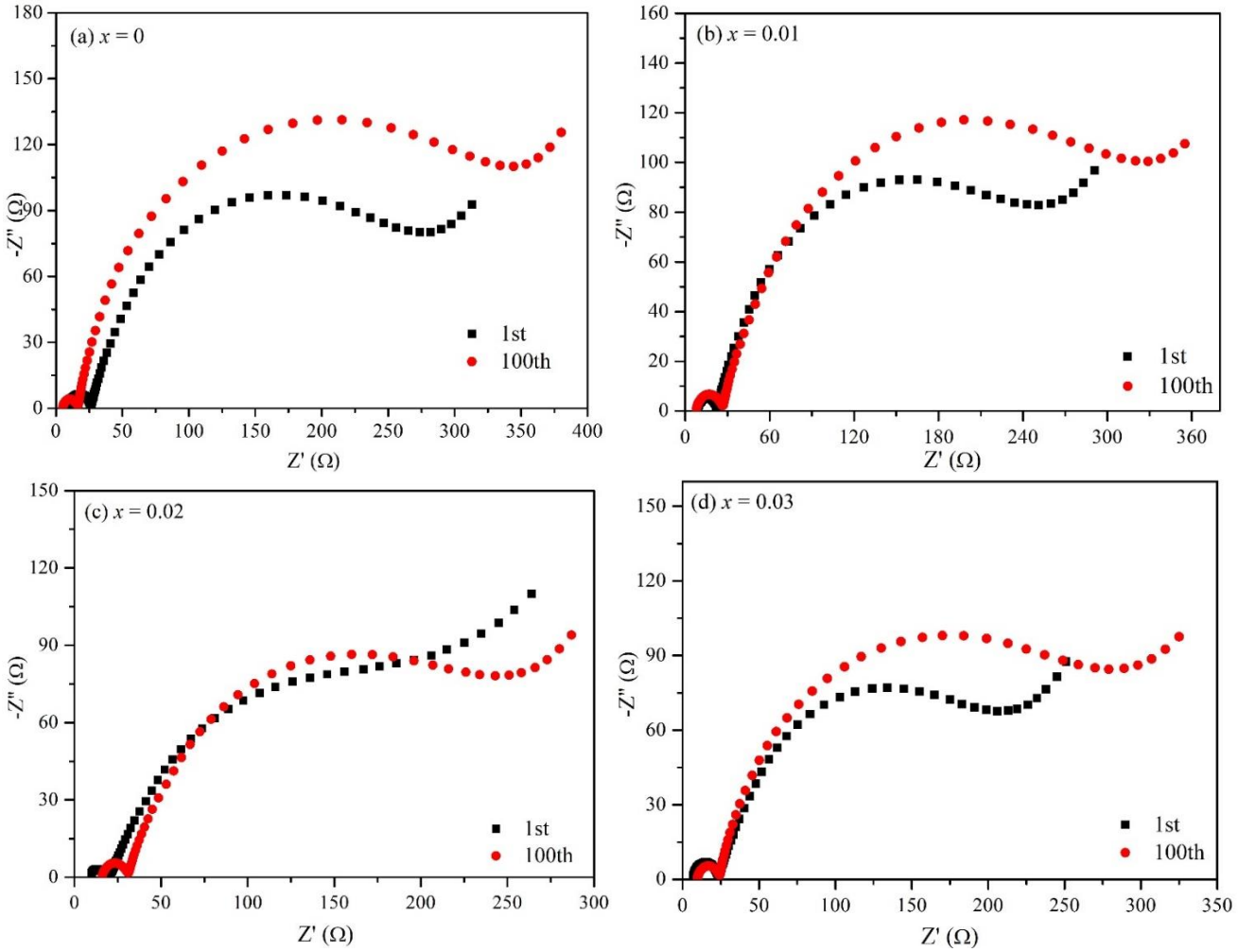

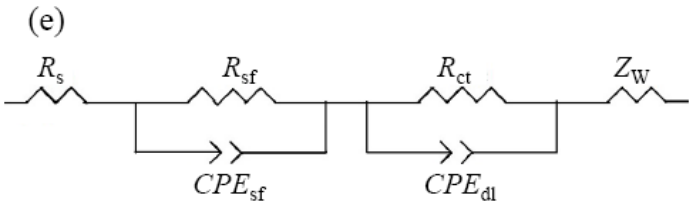

Figure 6. Nyquist plots of $Li_{1.20}[Mn_{0.54}Ni_{0.13}Co_{0.13}]_{0.8-x}Nb_xO_2$ (x = 0, 0.01, 0.02, 0.03) at different cycles (a)~(d); equivalent circuit performed to fit the Nyquist curves (e);

To further study the influence of Nb^{5+} doping on the kinetics of Li^+ insertion/extraction into $Li_{1.20}[Mn_{0.54}Ni_{0.13}Co_{0.13}]O_2$. The electrochemical impedance spectroscopy (EIS) for $Li_{1.20}[Mn_{0.54}Ni_{0.13}Co_{0.13}]_{0.8-x}Nb_xO_2$ (x = 0, 0.01, 0.02, 0.03) have been measured at different cycles, as is shown in Fig.6. All Nyquist plots have been fitted by an equivalent circuit model, as seen in Fig. 6(e). The intercept of the semicircle in the highest frequency region with the real axis (Z') is related with the ohmic resistance of whole cell (R_s). The semicircle at high-frequency is correlated with the impedance of Li^+ migration across the SEI film (R_{sf}). The semicircle in the high to medium frequency is relevance of the charge transfer resistance (R_{ct}). The quasi-straight line in the low frequency corresponds to the impedance of Li^+ diffusion in the bulk (W) [37, 38]. The fitting resistance values for all samples are shown in Table 7. In the 1st cycle, the cathodes after Nb^{5+} doping have demonstrated the lower values of R_s, R_{sf}, R_{ct} than those of the pristine one, proving the superior first discharge capacities for the Nb^{5+}-doped cathodes. After 100 cycles, the increase of R_{ct} for all cathodes are relatively large in comparison with the R_{sf}, implying that the cathode impedance is mainly expressed by the charge-transfer resistance. It can be seen that with the Nb^{5+} doping contents increasing, the $Li_{1.20}[Mn_{0.54}Ni_{0.13}Co_{0.13}]_{0.8-x}Nb_xO_2$ (x = 0.01, 0.02, 0.03) deliver the $\triangle R_{ct}$ values of 330.7, 261.2 and 289.6 Ω, smaller than that (423.0Ω) of the pristine one after 100 cycles. The results indicate that the Nb^{5+} doping restrain the increase of charge transfer resistance, and contributing to enhancing the electrochemical properties.

4. CONCLUSION

A typical carbonate co-precipitation method was adopted to synthesize the $Li_{1.20}[Mn_{0.54}Ni_{0.13}Co_{0.13}]_{0.8-x}Nb_xO_2$ (x = 0, 0.01, 0.02, 0.03) cathode materials. The XRD results indicated that the synthesized cathodes contain the $LiNi_{1/3}Co_{1/3}Mn_{1/3}O_2$ phase and Li_2MnO_3 phase. The SEM results showed that the size of the cathode particles decreased with Nb^{5+} doping content increasing, contributing to enhancing the discharge performance. The electrochemical tests further verified that the cathodes after Nb^{5+} doping demonstrated the superior cyclic performance, rate capacities and less initial irreversible capacity loss than those of the pristine one. Among all samples, the $Li_{1.20}[Mn_{0.54}Ni_{0.13}Co_{0.13}]_{0.78}Nb_{0.02}O_2$ delivered the optimal integrated electrochemical properties. Notably, it showed a high discharge capacity of 111.7 mAh g^{-1} at 5C high rate, which is larger than 91.1 mAh g^{-1} for the pristine one. Besides, an enhanced capacity retention of 92.5% after 100 cycles at 0.5C rate was obtained for $Li_{1.20}[Mn_{0.54}Ni_{0.13}Co_{0.13}]_{0.78}Nb_{0.02}O_2$, while the pristine cathode only delivered a capacity retention of 85.7%. The enhanced electrochemical properties for the Nb^{5+} doped cathodes could be attributed to the lower cation mixing and less amplification of charge transfer resistance during cycling.

ACKNOWLEDGEMENTS
We thank Zhang Yin for technical assistance. This work was supported by National Natural Science Foundation of China (Grant No. 3020050321328).

References

1. X.H. Liang, Y.C. Zhao, D. Han, J. Mao, L.X. Lan, *Int. J. Electrochem. Sci.*, 14 (2019) 717.
2. W. Li, B. Song, *Chem. Soc. Rev.* 46 (2017) 3006.
3. S. Kalluri, M. Yoon, M. Jo, S. Park, S. Myeong, J. Kim, S.X. Dou, Z. Guo, J. Cho, *Adv. Energy Mater.*, 7 (2016) 1601507.
4. C.Y. Zhu, J.X. Liu, X.H. Yu, Y.J. Zhang, X.D. Jiang, P. Dong, Y.N. Zhang, *Int. J. Electrochem. Sci.*, 14 (2019) 7673.
5. L.J. Chen, W.J. Feng, Z.S. Pu, X. Wang, W.X. Su, M.M. Li, C.K. Song, Z.J. Shi, Y.F. Zheng, *Int. J. Electrochem. Sci.*, 14 (2019) 8048.
6. Z.Y. Li, H.L. Zhang, *Int. J. Electrochem. Sci.*, 14 (2019) 3524.
7. M. Wang, M. Luo, Y.B. Chen, L. Chen, S. Yan, Y.Z. Ren, M. Chu, *J. Alloys Compd.*, 696 (2017) 891.
8. M. Wang, M. Luo, Y. Chen, Y. Su, L. Chen, R. Zhang, *J. Alloy Compd.*, 696 (2017) 907.
9. B. Seteni, N. Rapulenyane, J.C. Ngila, S. Mpelane, H. Luo, *J. Power Sources*, 353 (2017) 210.
10. B. Liu, Z. Zhang, M. Wu, S. Xu, *Int. J. Electrochem. Sci.*, 13 (2018) 7578.
11. L. Zhou, Y. Wu, J. Huang, X. Fang, T. Wang, W. Liu, Y. Wang, Y. Jin, X. Tang, *J. Alloys Compd.*, 724 (2017) 991.
12. M. Wang, M. Luo, Y. Chen, Y. Su, L. Chen, R. Zhang, *J. Alloy Compd.*, 696 (2017) 907.
13. B.W. Xiao, B.Q. Wang, J. Liu, K. Kaliyappan, Q. Sun, Y.L. Liu, G. Dadheech, M.P. Balogh, L. Yang, T.K. Sham, R.Y. Li, M. Cai, X.L. Sun, *Nano Energy*, 34 (2017) 120.
14. C. Song, W. Feng, W. Su, L. Chen, M. Li, *Int. J. Electrochem. Sci.,* 14 (2019) 2372.
15. F. H. Zheng, X. Ou, Q.C. Pan, X. H. Xiong, H. C. Yang, M.L. Liu, *J. Power Sources*, 346 (2017) 31.
16. X. Chang, Q. Xu, X. Yuan, C. Lai, H. Liu, *Int. J. Electrochem. Sci.*, 12 (2017) 10071.
17. K. Xie, J. Qian, Y. Zhou, Z. Chen, Y. Lin, F. Chen, Z. Shen, *Powder Technology*, 339 (2018) 838.
18. Y. Lu, M. Pang, S. Shi, Q. Ye, Z. Tian, T. Wang, *Sci. Rep. UK*, 8 (2018) 2981.
19. J. Lee, D.A. Kitchaev, D.-H. Kwon, C.-W. Lee, J. K. Papp, Y.-S. Liu, Z. Lun, R.J. Clément, T. Shi, B.D. McCloskey, J. Guo, M. Balasubramanian, G. Ceder, *Nature*, 556 (2018) 185.
20. Y. Lu, S. Shi, F. Yang, T. Zhang, H. Niu, T. Wang, *J. Alloy Compd.*, 767 (2018) 23.
21. G. Li, X. Liu, Y. Zhao, Z. Shao, *Int. J. Electrochem. Sci.*, 13 (2018) 7321
22. H. Meng, L. Li, J. Liu, X. Han, W. Zhang, X. Liu, Q. Xu, *J. Alloy Compd.*, 690 (2017) 256.
23. W. Pan, W. Peng, H. Guo, Jiexi Wang, Zhixing Wang, Hangkong Li, Kaimin Shi, *Ceram. Int.*, 43 (2017) 14836.
24. X. Li, L. Zheng, Z. Zang, T. Liu, F. Cao, X. Sun, S. Sun, Q. Niu, Y. Lu, T. Ohsaka, J. Wu, *J. Alloy Compd.*, 744 (2018) 41.
25. D. Luo, S. Fang, L. Yang, S. Hirano, *J. Alloy Compd.*, 723 (2017) 243.
26. L. Ming, B. Zhang, Y. Cao, J.-F. Zhang, C.-H. Wang, X.-W. Wang, H. Li, *Front. Chem.*, 6 (2018) 76
27. L. Zhao, Q. Wu, J. Wu, *J. Solid State Electrochemistry*, 22 (2018) 2141-2148.
28. R.J. Diao, G.P. Nayaka, C.Y. Zhu, X.H. Yu, Y.N. Zhang, J. Rong, X. Wang, Y.J. Zhang, P. Dong, M.Y. Zhang, X. Yang, Z.L. Zhan, *Int. J. Electrochem. Sci.*, 14 (2019) 8070.
29. Y. Zhou, Y. Wang, S. Li, J. Mei, H. Liu, H. Liu, G. Liu, *J. Alloys Compd.*, 695 (2017) 2951.
30. M. Xu, L. Fei, W. Lu, Z. Chen, T. Li, Y. Liu, G. Gao, Y. Lai, Z. Zhang, P. Wang, H. Huang, *Nano Energy*, 35 (2017) 271.
31. R.M. Yang, Y.J. Zhang, P. Dong, Y.N. Zhang, *Int. J. Electrochem. Sci.*, 13 (2018) 8116.
32. Z. Q.Deng, A. Manthiram, *J.Phys. Chem. C*, 115 (2011) 7097.
33. K. Karthikeyana, S. Amaresha, G.W. Lee, V. Aravindana, H. Kim, K.S. Kang, W.S. Kim, Y.S. Lee, *Electrochim. Acta*, 68 (2012) 246.

34. M. Lou, S.-S. Fan, H.-T. Yu, Y. Xie, Q. Zhang, Y.-R. Zhu, T.-F. Yi, G.-H. Tian, *J. Alloys Compd.*, 739 (2018) 607.
35. K. Wu, G. Jia, X. Shangguan, G. Yang, Z. Zhu, Z. Peng, Q. Zhuge, F. Li, X. Cui, *J. Alloys Compd.* 765 (2018) 700.
36. C.P. Laisa, R.N. Ramesha, K. Ramesha, *Electrochim. Acta*, 256 (2017) 10.
37. D. Luo, S. Fang, L. Yang, S. Hirano, *J. Alloy Compd.*, 723 (2017) 243.
38. D. Zhang, W. Li, N. Li, J. Qiao, Z. Ma, C. Chang, *Int. J. Electrochem. Sci.*, 13 (2018) 6402.